INTERNATIONAL ATOMIC ENERGY AGENCY
UNITED NATIONS EDUCATIONAL, SCIENTIFIC AND CULTURAL ORGANIZATION
INTERNATIONAL CENTRE FOR THEORETICAL PHYSICS
I.C.T.P., P.O. BOX 586, 34100 TRIESTE, ITALY, CABLE: CENTRATOM TRIESTE

UNITED NATIONS INDUSTRIAL DEVELOPMENT ORGANIZATION
INTERNATIONAL CENTRE FOR SCIENCE AND HIGH TECHNOLOGY

SMR: 630/5

MINIWORKSHOP ON NONLINEARITY: Dynamics of Surfaces in Nonlinear Physics

(13 - 24 July 1992)

"Turbulence in Helium-Gas Free Convection"

presented by:

A. Libchaber
NEC Research Institute
4 Independence Way
Princeton, NJ 08540
U.S.A..

PHYSICAL REVIEW A VOLUME 40, NUMBER 11 DECEMBER 1, 1989

Turbulence in helium-gas free convection

Masaki Sano,* Xiao Zhong Wu, and Albert Libchaber
The James Franck Institute and The Enrico Fermi Institute, The University of Chicago, 5640 South Ellis Avenue
Chicago, Illinois 60637

(Received 5 June 1989)

Results on a Rayleigh-Bénard experiment in helium gas at 5 K in a cylindrical cell of aspect ratio 1 are presented. The Rayleigh number spans a range from 10^5 to 10^{12}. A large-scale coherent flow is observed via the correlation of two adjacent temperature probes. This flow-velocity measurement shows clear transitions between different turbulent states. In hard turbulence, the dimensionless velocity $[V/(\kappa/L)]$ scales with the Rayleigh number, with an exponent close to $\frac{1}{2}$. The horizontal temperature difference across the cell is another measure of the different turbulent states. The temperature signals in the side-wall region (the large mean vertical velocity region) give clear pictures of various turbulent states. The measured velocity has been compared with the calculated free-fall velocity and also the heat transfer rate with the one calculated from the flow advection. The coherent frequency ω_p is found to be associated with the large-scale flow. In the side-wall region the power spectrum of the local temperature signal has a power-law dependence for Rayleigh numbers between 10^8 and 10^{11}. Both the exponent and the range of the power law change with the Rayleigh number. For Rayleigh numbers above 10^{11}, a power law independent of Rayleigh number (exponent 1.4) develops at low frequency.

I. INTRODUCTION

In this paper we present results on the turbulent convection of helium gas at low temperature. We concentrate on two main aspects of the heat transfer: first, the large-scale flow in the experimental cell and second, the large-scale horizontal temperature difference. A power-law relation with the Rayleigh number is found for the large-scale velocity and for the horizontal temperature difference in the hard-turbulence regime. These results confirm our previously proposed classification of various dynamical states and help to elucidate some of the characteristics of those regimes. They also lead to some pertinent questions related to the scaling model proposed previously. Finally, a study of the inertial and dissipative range of turbulence, through fast Fourier spectrum analysis of the local temperature, leads to unexpected results. They may be related to the problem of injection from the thermal boundary layers.

In free thermal convection, the control parameter is the Rayleigh number R defined as

$$R = \frac{\alpha g L^3 \Delta}{\nu\kappa} , \tag{1}$$

where α is the isobaric thermal expansion coefficient, g is the acceleration of gravity, L is the height of the cell, Δ is the temperature drop from the bottom to the top plate of the cell, ν is the kinematic viscosity, and κ is the thermal diffusivity. ν and κ can be small for low-temperature gas and varied in a wide range by changing the gas density. α is large for a low-temperature gas. Evidently, helium gas is the one that can reach the coldest temperature. These features of low-temperature helium gas made it possible for Threlfall[1] to study thermal convection in a wide range of Rayleigh numbers (up to 10^{10}).

The first results on this experiment was reported by Heslot, Castaing, and Libchaber.[2] They discovered different turbulent states, which were denominated as soft and hard turbulence. The transition from soft to hard turbulence occurs at $R = 4 \times 10^7$ for the experimental cell of aspect ratio 1. Hard turbulence is distinguished from soft turbulence by the distribution function of the temperature signal in the center region of the cell. The distribution function in hard turbulence is exponential and that of soft turbulence is Gaussian. Hard turbulence is also characterized by the appearance of a coherent frequency ω_p of finite width, present in all parts of the cell. Castaing *et al.*[3] further reported that all the statistical quantities in hard turbulence scale as power laws of the Rayleigh number. Also, all the exponents in it have been compared with a scaling theory, which introduces a third length scale (the mixing length scale) besides the size of the cell L and the thermal boundary layer thickness δ. In a study of soft turbulence, Wu *et al.*[4] reported that the Nusselt number of this state satisfies the classical $R^{1/3}$ law, and the characteristic time scales as $R^{-2/3}$, which follows Malkus[5] and Howard[6] results (the Nusselt number N is defined as the heat transfer rate normalized by that calculated from conduction; it is unity when the gas is in pure conduction state).

All the previous studies[2-4] on this experiment concentrate on the global physical quantities and the behavior of the center region, where the turbulent flow is regarded as homogeneous. Krishnamurti and Howard[7] observed stable coherent large-scale motion in a thermal convection cell of a large aspect ratio. We expect such motion to be present in our experiment. The large scale motion would create a new region in the cell near the lateral boundary region. In order to understand the global behavior of the turbulent motion in the cell, it is necessary to study this region and understand how it matches with the motion of the other parts of the cell.

In this paper, we study the large-scale flow in the cell. The experiment is described briefly in Sec. II. We discuss the velocity measurement technique in detail in Sec. III. The measurement of the vertical velocity is presented and the new region is characterized as the side-wall region of a large mean vertical flow velocity. As we shall see in Sec. IV, the transition from soft to hard turbulence and the distinction between the two substates of soft turbulence are clearly observed in the temperature signal of the side-wall region. In Sec. V, we discuss the histograms and power spectra of the temperature signals, which are different from those of the center region, but asymptotically approach them as the Rayleigh number increases. Some unique features of the power spectrum are reported. Finally, in Sec. VI we critically assess our experimental results and discuss the shortcoming of the proposed model.[3]

II. EXPERIMENT

The experimental set up has been detailed in previous papers[2,3] so we mention only the essential points here. The experimental cell is a vertical cylinder of aspect ratio 1, diameter 8.7 cm. The top and the bottom plates are made of oxygen-free high-conductivity copper, which can achieve thermal homogeneity rapidly due to its large thermal conductivity at low temperature. The side wall is made from stainless steel of about 1-mm thickness. Given the stainless-steel thermal conductivity of 2×10^{-3} W cm^{-1} K at 5 K, the heat transported by the side wall is small, comparable to the heat conduction of the helium gas in the cell. We subtract the heat conducted by the side wall from the total heat transported in the Nusselt number calculation. The cell is surrounded by a vacuum jacket, which sits in a liquid-helium bath. The top plate of the cell and the top plate of the vacuum jacket sandwich a thin aluminum cylinder with two indium *O* rings on its two ends. Such a structure creates a well-defined and reasonable thermal resistance between the top plate of the cell and the liquid-helium bath. We heat the bottom plate with a dc current through a resistance wire and regulate the top plate to a temperature of about 5 K. The temperature drop across the cell Δ ranges from about 50 to 700 mK with properly set heating current. The Rayleigh number and the Nusselt number are measured.

Most of the analyses in this paper are based on local temperature measurements. The bolometers are arsenic doped silicon cubes of about 0.2 mm. At the middle height of the cell, two parallel 0.1-mm-diam manganin wires (about 1 cm apart) span horizontally across the center of the cell. The bolometers are supported by their electrical leads of 10 μm diam, which lay on these two manganin wires (see Fig. 1). We fixed the pairs at 2.5, 4, 5, 10, 24, and 31 mm away from the side wall, respectively (we call them *A*, *B*, *C*, *D*, *E*, *F*, and *G*, correspondingly). Each pair consists of two bolometers placed about ~2 mm apart vertically. A single bolometer (we call it *D*′) was also fixed at a point that is axis symmetric to that of the pair *D* (10 mm away from the side wall). The signal at the center of the cell was also measured with a single bolometer.

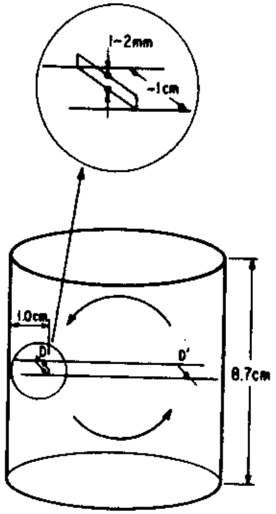

FIG. 1. Bolometers of the *D* pair and the *D*′ bolometer are supported by two wires in the middle height of the convection cell. The other pairs of bolometers are in the same side of the *D* pair. The arrow shows the direction of the large-scale flow.

Signals from the bolometers in each pair are measured simultaneously by a two channel HP 3652 dynamical signal analyzer. For each signal, we take two time series, one of about 4×10^5 digitized points sampled with the frequency of 2.56 times the maximum observed frequency, which is about 200 Hz, and another one of longer time of about 1 h, with a frequency of about one-fifth of the maximum. The longer time scale measurements are made in

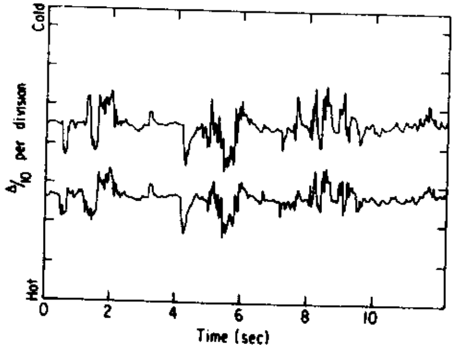

FIG. 2. Typical hard-turbulence signals by the *D* pair bolometers. They are the same in the lower-frequency component except for a time delay. The direction of the temperature axis is labeled by "hot" and "cold."

order to achieve better statistics for the low-frequency part of the measurement. Signals of the paired bolometers are identical in the lower frequency domain except for a time delay (Fig. 2). The mean vertical velocity can be deduced from the time delay.

Figure 3 shows four typical signals of one of the *D* pair bolometers at the Rayleigh numbers 2.0×10^5, 5.7×10^5, 5.5×10^6, and 5.0×10^{10}. The curves (a), (b), (c), and (d) are, respectively, in the transition region from chaos to turbulence ($1\times10^5<R<3\times10^5$), the first soft-turbulent state ($3\times10^5<R<5\times10^6$), the second soft-turbulent state ($5\times10^6<R<4\times10^7$) and the hard-turbulent state ($4\times10^7<R$). In each plot, there are 10 240 points sampled at the frequency of 2.56 times the maximum frequency observed. The direction of the temperature axis is indicated by the labels "hot" and "cold."

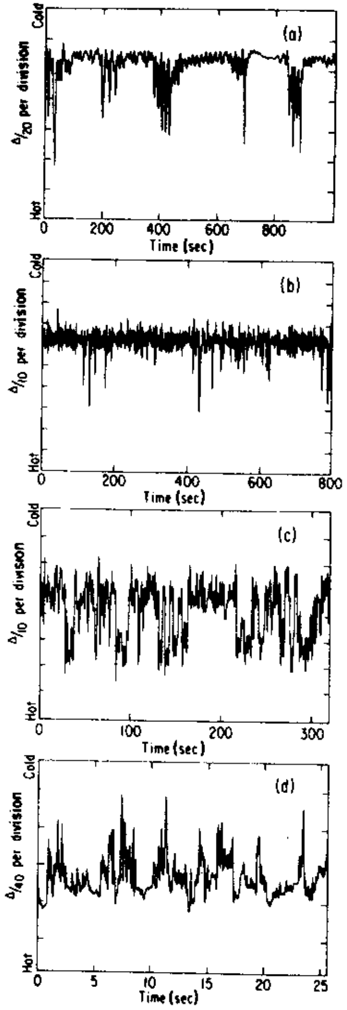

FIG 3. Typical signals by one bolometer of the *D* pair at the Rayleigh number (a) 2.0×10^5, (b) 5.7×10^5, (c) 5.5×10^4, and (d) 5.0×10^{10}. In each plot, there are 10 240 points sampled at the frequency of 2.56 times the maximum frequency observed. Since the normalized amplitude of a signal changes with *R*, the unit of the temperature axis has to be adjusted such that the signal fits the full scale.

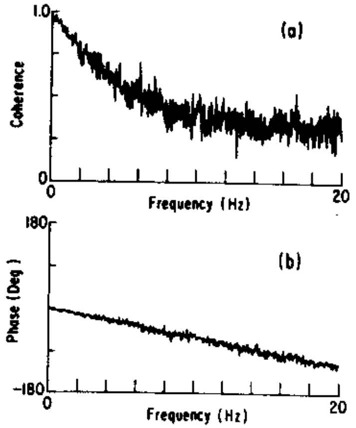

FIG. 4. (a) Coherence function between the signals from the bolometers of the *D* pair and (b) the phase of their cross spectrum.

We describe briefly the content of Fig. 3. As shown on Fig. 1, the bolometers of the *D* pair are placed in the descending part of the main circulation. In hard turbulence [Fig. 3(d)], cold fluctuations are seen superposed on an average base line, they are related to cold thermal plumes advected from the top boundary layer, and they arrive in groups at a frequency ω_p (about 5 sec). For lower Rayleigh numbers of Figs. 3(a) and 3(b), the fluctuation are bursts of opposite sign, i.e., hot fluctuation. They are associated to detachment of the boundary layer near the

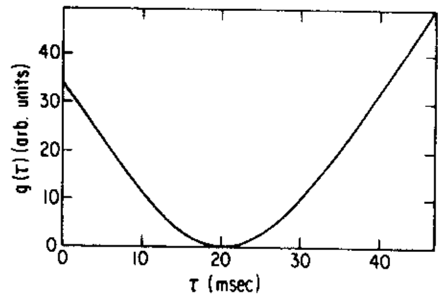

FIG. 5. The function $g(\tau)=\sum_i[T_1(t_i)-T_2(t_i-\tau)]^2$ has a minimum at τ_0, which is the delay time.

bottom corner of the cell, where the descending fluid experiences an adverse pressure effect. As the Rayleigh number increases, there are more and more bursts in the hot side, and they connect to form a two-level system at the end of soft turbulence [Fig. 3(c)].

III. LARGE SCALE VELOCITY

As we see in Fig. 2, the signals from paired bolometers are the same in the lower frequency domain except for a time delay. In order to see this more clearly, we measured the cross spectrum between them. The cross spectrum between two signals is the Fourier transform of their cross correlation. If two signals are identical except or a delay time τ_0, the phase of their cross spectrum is inear with the frequency with a slope $2\pi\tau_0$, and the coherence function is unity in all the frequency range coherence function is the amplitude of the cross spectrum normalized by the original power spectra). Figure (a) and 4(b) are the phase of the cross spectrum of the ctual signals from the paired bolometers and their oherence function. The phase is linear with the frequency and the coherence function is large in the same lower-requency domain. We conclude from these that there xists a mean vertical velocity with which the fluid passes rom one bolometer to another with its lower frequency otion unchanged.

As mentioned above, the slope of the phase of the cross pectrum is related to the delay time τ_0 by

$$2\pi\tau_0=\frac{d\phi}{df}\ , \tag{2}$$

here ϕ is the phase and f is the frequency. The delay me τ_0 can also be measured directly with the cross rrelation function, or with a related function. We callated

$$g(\tau)=\sum_i [T_1(t_i)-T_2(t_i-\tau)]^2\ , \tag{3}$$

here $T_1(t_i)$ and $T_2(t_i)$ are the temperatures measured the paired bolometers at time t_i. We find τ_0 by minimng $g(\tau)$ (Fig. 5.). This method will give an unambigus delay time even when the phase of the cross spectrum ot strictly linear, which is sometimes the case for soft bulence. As a matter of fact, the methods by the ase and the correlation give the same result except that latter has smaller scatter.

t has been visualized in a thermal convection cell of ter by Gross, Zocchi, and Libchaber[8] that the horizonvelocity V_h is much smaller than the mean vertical veity V_z in the side-wall region. Therefore V_z is related he delay time τ_0 approximately by

$$\tau_0=\frac{d}{V_z}\ , \tag{4}$$

re d is the vertical spacing of the paired bolometers. wever, if we are interested in the precise scaling law of velocity with the Rayleigh number, we cannot ignore horizontal velocity V_h even in the side-wall region, to mention the intermediate region between the side-region and the center region. The modified relation between τ_0 and the velocity is

$$\tau_0=\frac{d}{(V_z^2+V_h^2)^{1/2}}\frac{V_z}{(V_z^2+V_h^2)^{1/2}}\ , \tag{5}$$

where $V_z/(V_z^2+V_h^2)^{1/2}$ is the correction factor due to the flow direction. It is plausible to assume in the hard-turbulence regime that V_z and V_h have the same scaling relation with the Rayleigh number. Therefore Eq. (4) will still give the correct velocity scaling with the Rayleigh number, although the actual magnitude of the vertical velocity can not be trusted with great precision. From now on, we shall calculate the velocity from Eq. (4) and simply denote it as V. The direction of the vertical velocity can be decided by the sign of the delay time and the relative position of the paired bolometers.

The measurement of all the seven pairs of bolometers and the single bolometer D' have been performed in three runs (D and D' were in the same run). The velocities at each run are repeatable: the normalized velocity $V/(\kappa/L)$ at each position is only dependent on the Rayleigh number, and the flow direction on the side of the paired bolometers is always downward. The histogram of the temperature fluctuation by the single bolometer D' skews to the opposite side of that of each of the paired bolometers. This indicates that the large scale flow is a one roll structure, i.e., the fluid moves upward on one side and downward on the opposite side. Evidently, a symmetry-breaking mechanism is responsible for the flow direction. We found that a cell's inclining by about 2° may change the flow direction. We do not know if this is relevant in our case or if the symmetry breaking comes from other small defects of the cell.

Figure 6 is the plot of the normalized velocity $V/(\kappa/L)$ measured by the pair D as a function of the Rayleigh number. Since ν is close to κ, $V/(\kappa/L)$ is the Reynolds number scaled to the cell height L. Three regions appear clearly as the first soft turbulence $(3\times10^5<R<3\times10^6)$, the second soft turbulence $(3\times10^6<R<4\times10^7)$, and hard turbulence $(4\times10^7<R)$. The normalized velocities measured by all the seven pairs have scaling relations with the Rayleigh number in the hard-turbulence region. The velocity in the soft-turbulence region is not perfectly reproducible, i.e., the normalized velocities vary from run to run. We think that the large-scale flow is not well locked in soft turbulence. However, $V/(\kappa/L)$ versus R of all the seven pairs have kinks at $R=3\times10^6$ and $R=4\times10^7$ showing the transitions, although the detailed signatures may be different.

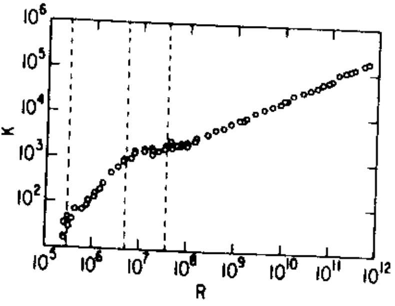

FIG. 6. Normalized velocity $V/(\kappa/L)$ measured by the bolometers of the D pair as a function of the Rayleigh number.

Although the magnitude of the velocity measurement is not precise, we can have a qualitative vertical velocity profile from the measurements. The velocity should be zero at the side wall because of the nonslip boundary condition, and it will reach a maximum value out of the viscous boundary layer. In this experiment, the velocity reaches its maximum value at about 10 mm away from the side wall. It decreases gradually when moving out of the side-wall region and into the center. We believe that the mean velocity goes asymptotically to zero in the center region.

In hard turbulence, $V/(\kappa/L)$ scales with the Rayleigh number $V/(\kappa/L)=CR^\gamma$, and we determined the exponents γ for the seven pairs. Figure 7 is a plot of this exponent as a function of the distance. The exponent decreases as one goes toward the center region, and it saturates at 0.485 for pairs more than 10 mm away from the side wall. Since the side-wall-region width shrinks as the Rayleigh number increases, a pair of bolometers in the side-wall region will change its position with respect to the velocity profile. Therefore, the dependence of the measured velocity on the Rayleigh number is the combined effect of the dependence on the Rayleigh number of both the velocity itself and the side-wall-region width. However, the velocity measured outside the side-wall region is free from this effect and its scaling is the scaling of the velocity alone. As shown if Fig. 7, the exponent starts to level at 1 cm, the side-wall region is therefore estimated as about 1 cm. For the D pair, which is 1 cm away from the side wall, we obtain

$$\frac{V}{\kappa/L}=0.309R^{0.485\pm0.005}\ .$$

The exponent 0.485 is then the scaling exponent for the velocity.

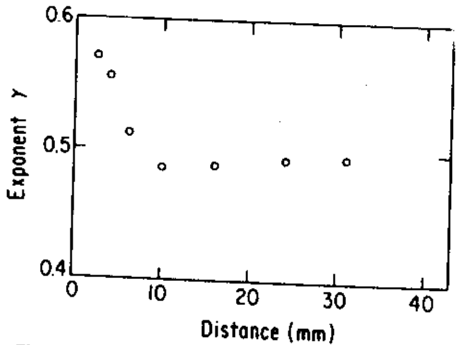

FIG. 7. The exponent of the scaling relation between $V/(\kappa/L)$ and the Rayleigh number is plotted as a function of the distance. The distance is zero at the side wall and 43 mm at the center of the cell.

IV. HORIZONTAL TEMPERATURE GRADIENT AT THE MIDDLE HEIGHT

In the first run, we measured the signals of one of the D pair bolometers and the D' bolometer at the same time. As we mentioned above, the positions of D and D' are 10 mm away from the side wall and axis symmetric to each other. The temperature distribution function, i.e., the histogram measured by D' is a mirror image of that measured by D. The power spectra measured by D and D' are almost identical. This complete antisymmetry of their histograms and the identity of their power spectra indicate that the flow on the two opposite sides is the same, but of opposite directions.

We measured the average temperature on the two sides. The average temperature at the side of the D' bolometer is higher than the average temperature of the whole cell (which is the average of the top and bottom plate temperature), while that of the other side is lower. Figure 8(a) shows the difference of the average temperature (normalized by Δ) at the two sides as a function of the Rayleigh number. The root-mean-square (rms) temperature fluctuation $T_{\rm rms}$ measured by one of the D pair bolometers, after being normalized by Δ, is plotted in Fig. 8(b). In Fig. 8(a), several transition points between different turbulent states are clearly visible at the Rayleigh numbers of 3×10^5, 5×10^6, and 4×10^7. Those states are the transition region from chaos to turbulence, the first and the second soft-turbulent states and hard-

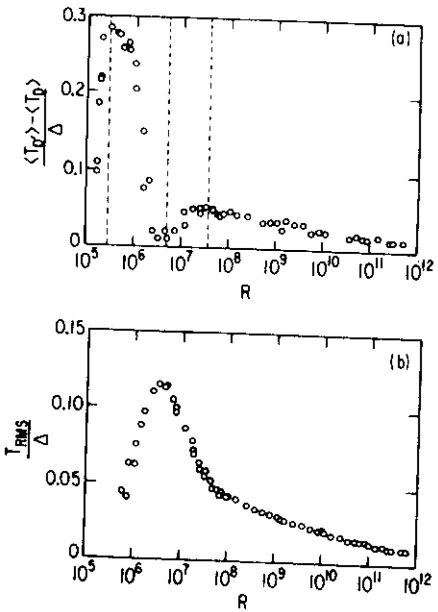

FIG. 8. (a) horizontal temperature difference and (b) the rms of the temperature fluctuation $T_{\rm rms}$, normalized by Δ, as function of the Rayleigh number.

turbulent state, respectively. Their typical temperature signals have already been shown in Fig. 3.

Let us first describe the transition region from chaos to turbulence ($1\times10^5 < R < 3\times10^5$). The horizontal temperature difference and the rms of the temperature fluctuation $T_{\rm rms}/\Delta$ increase rapidly with the Rayleigh number. The temperature difference even reaches a maximum value of about 30% of Δ. The signal from bolometers of the D pair is characterized by abrupt hot bursts on the basis of the rather quiet motion of cold fluid [Fig. 3(a)]. This is a regime where the large-scale motion leads to hot fluid going up on one side and cold fluid going down on the opposite side. This was observed by Chu and Goldstein[9] in visualizing thermal convection in water, leading to a vertical temperature inversion. The hot fluctuations in the descending flow [Fig. 3(a)] are due to the detached boundary layers. As the descending flow reaches the bottom plate, the abrupt change of the flow direction causes an adverse pressure gradient, which then leads to the detachment of the boundary layer.[10,11]

In the region of $3\times10^5 < R < 5\times10^6$, the horizontal gradient decreases and the rms of the temperature fluctuation $T_{\rm rms}/\Delta$ keeps increasing as the Rayleigh number increases. The signal is characterized by more abrupt bursts of hot fluctuation on a rougher background motion [Fig. 3(b)]. It is a regime where the hot and cold fluids are more efficiently mixed with the surrounding fluid by the more turbulent motion as the Rayleigh number increases. Thus the temperature difference decreases as the Rayleigh number increases. On the other hand, the more turbulent fluid motion at a higher Rayleigh number will create a larger rms of the temperature fluctuation.

In the region of $5\times10^6 < R < 4\times10^7$, more and more bursts appear in the signal that eventually connect together. The signal is finally characterized by its clear two-level switching, with one level being the original background motion and another level being the connection of the bursts [Fig. 3(c)]. We propose that the detached boundary layers form secondary rolls. The back flow of hot fluid has higher temperature than that of the large scale motion, which leads to the two-level switching. The slight increase of the horizontal temperature with the Rayleigh number may be due to the change of the flow structure on the two sides.

As the Rayleigh number goes beyond 4×10^7, it gets into hard turbulence [Fig. 3(d)]. The signal is more intermittent. The rms of the temperature fluctuation $T_{\rm rms}/\Delta$ decreases with a power law as the Rayleigh number increases. The horizontal temperature difference exhibits the same dependence on the Rayleigh number as the rms of the temperature fluctuation. The main observation in Fig. 3(d) is that the sign of the temperature fluctuation reverses, this indicates that a new mechanism sets in. The thermal boundary layers nucleates thermal plumes, those plumes are advected by the flow, as visualized in water (Gross, Zocchi, and Libchaber[8] Chu and Goldstein[9]), and this leads to cold fluctuations for descending flows. Those plumes are the major source for the temperature fluctuation and the horizontal temperature gradient.

The conclusion is that emission of thermals explains the observed phenomena in hard turbulence, while for soft turbulence, the instability of the large scale flow in regions of adverse pressure gradient leads to fluctuations of the opposite sign. As shown in Fig. 1, cold plumes are advected to D from the top boundary layer in hard turbulence. In soft turbulence, instability of the thermal boundary layer at the bottom of the cell leads to hot fluctuation.

V. HISTOGRAM AND THE POWER SPECTRUM

The turbulence in the cell can be viewed as having three different sections in radial direction. The viscous boundary layer, which will not exceed $\sqrt{\nu L/V}$, is smaller than a few millimeters (the typical velocity V is 10 cm/sec, ν varies from 10^{-1} to 10^{-4} cm^2/sec, and L is 8.7 cm). Apparently there is an asymptotically homogeneous and nearly isotropic center region, where the mean velocity is zero. Our experiment shows the existence of another region between the viscous boundary layer and the center region, and we call it the side-wall region. In the side-wall region, the velocity has a large mean vertical component and a relatively small horizontal component; the plumes therefore are mixed with the background flow less efficiently than in the center region. The large rms and skewness of the local temperature fluctuation are the signatures of the side-wall region. However, the side-wall region shrinks as the Rayleigh number increases, so the signal at any fixed point in the side-wall region will

asymptotically approach that of the center region. Figure 9 is the histograms of one of the D pair bolometers compared with those of the exact center for the same Rayleigh numbers in the typical turbulent states. The histograms for the exact center are Gaussian in soft turbulence [Figs. 9(a) and 9(b)] and are exponential in hard turbulence [Figs. 9(c) and 9(d)], as presented previously.[3] The histograms in the side-wall region do not have such a general behavior. The histogram of the first soft-turbulent state [Fig. 9(a′)] has a Gaussian distribution superposed with a long tail in the hot side. The histogram of the second soft-turbulent state [Fig. 9(b′)] has two broad peaks which correspond to the two levels in the time signal Fig. 3(c). Besides the signatures of different turbulent states, we can see that the histograms of the side-wall region asymptotically approach those of the center as the Rayleigh number increases [Figs. 9(c′) and 9(d′)].

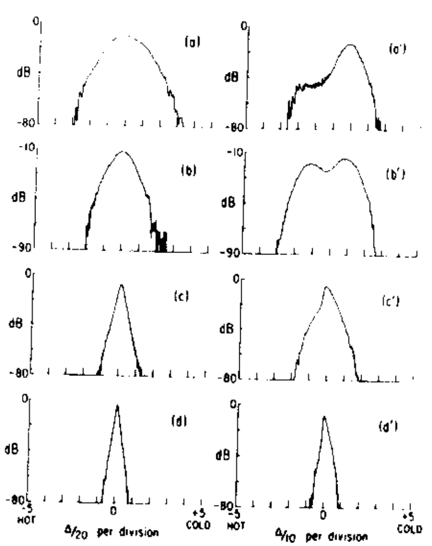

FIG. 9. On the left, the histograms of the bolometer at the exact center at the Rayleigh numbers (a) 1×10^6, (b) 5×10^6, (c) 1×10^8, and (d) 4×10^{10}. On the right, histograms of one of the D pair bolometers at the same Rayleigh numbers (a′), (b′), (c′), and (d′).

We finally discuss the power spectrum of the local temperature fluctuation in the side-wall region. Figure 10(a) is a power spectrum for $R = 3\times10^{10}$ measured by one of the D pair bolometers. The dotted curve is the fitting by

$$P(\omega) = \left[\frac{\omega}{\omega_0}\right]^{-s} \exp\left[-\frac{\omega}{\omega_h}\right], \tag{6}$$

with ω_0, s, and ω_h as parameters. We can see that there is a power law starting from the region above ω_p and extending more than two decades of the frequency. The fitting of the power law by the Eq. (6) is good for Rayleigh numbers between 10^8 and 10^{11}. For R below 10^8, the power spectrum simply does not have a power law. For R above 10^{11}, a single power law with an exponential cutoff can no longer fit the power spectrum at the low-frequency region just above ω_p. In Fig. 10(b), the power spectrum for $R = 2\times10^{11}$ is illustrated by two dotted lines representing two power laws. The exponent for the power law just above the ω_p is around 1.4, the same power law has been reported[2] in the power spectrum of the center bolometer.

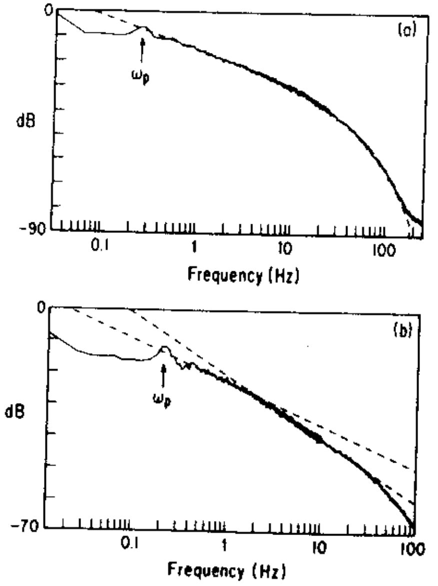

FIG. 10. A power spectrum of one bolometer of the D pair at $R = 3\times10^{10}$. The dashed line is the fitting curve by $P(\omega) = (\omega/\omega_0)^{-s}\exp(-\omega/\omega_h)$. (b) The power spectrum for $R = 2\times10^{11}$. It is illustrated by two power laws.

In the range of $10^8 < R < 10^{11}$ the power law of the power spectrum starts from ω_p. The power spectrum of each of the A, B, C, and D pair of bolometers has a fairly good fit to the Eq. (6). For the same Rayleigh numbe the fitted exponents s for all the bolometers of the 6 pairs are the same, within the fitting uncertainty. Even the fitted exponent of the power spectrum of each of the E, F, and G pairs, for which the fitting is only good in a narrow Rayleigh number range around 10^{10}, is the same as that of others. Figure 11 is the plot of the fitted exponent s as a function of the Rayleigh number. It is surprising that the exponents s of the power law in the power spectrum changes with the Rayleigh number from about 0.8 to about 1.5. The changing of the power law suggests that turbulence in the thermal convection may not be as simple as the theory proposed by Kolmogorov.[12] The exponential cutoff frequency ω_h, normalized by κ/L^2, scales as $R^{0.70\pm0.05}$ in average. For the D pair specifically,

$$\frac{\omega_h}{\kappa/L^2} = 0.010R^{0.74\pm0.02} .$$

The power-law range of the power spectrum is betwe ω_h and ω_p, whose scaling with Rayleigh number has be measured previously[3] as

$$\frac{\omega_p}{\kappa/L^2} = 0.36R^{0.491\pm0.002} .$$

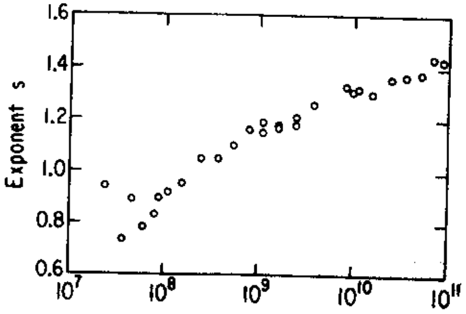

FIG. 11. Fitted exponent s of the power law in the power spectrum as a function of the Rayleigh number ($R < 10^{11}$).

VI. DISCUSSION

The presence of the large-scale coherent flow was not considered in the previous paper,[3] although it plays a crucial role in turbulent thermal convection. In this paper, we present measurement on the large-scale flow. Taking it into account, one obtains a better understanding of some aspects of turbulent convection, such as oscillations at the frequency ω_p, and the transitions among the different states.

In Sec. VI A, quantitative comparisons between theoretical estimates and the measurement for the velocity and the heat transport are presented. In order to compare the scaling exponent of velocity with existing theories, the Prandtl number dependence of the velocity scaling needs to be considered. This is discussed in Sec. VI B. In Sec VI C, the relation between large-scale flow and the other observed phenomena, such as the oscillations at the frequency ω_p and transitions among the states, are discussed.

A. Free-fall velocity and heat transport

Large-scale flow in turbulent convection was first observed by Krishnamurti and Howard.[7] Fitzjarrald[13] found that heat transfer in the thermal convection system is dominated by large-scale structure. However, its mechanism and quantitative aspect remained open. Here we try to extend the scaling argument[3] of fluctuating velocity and heat transfer in the center region to the large-scale flow. Velocity and heat transfer can be estimated from the measurements of other physical quantities and will be compared with the direct measurements.

For high enough Reynolds number one can neglect the dissipation effect at large length scale. Under this condition, the velocity will be a free-fall velocity V_f,

$$V_f \approx (\alpha g T_{\rm rms} L)^{1/2} . \tag{7}$$

As described in Sec. III, the Reynolds number based on the cell size ranges from 10^3 to 10^6 in the hard-turbulence regime. For such high Reynolds number, the assumption of free-fall velocity is justified.

The Nusselt number can also be estimated from the measurements of other physical quantities. For high enough Nusselt number, heat is transported only by advection in the middle height region and is then $T_{\rm rms}V$. The corresponding Nusselt number $N_{\rm adv}$ is

$$N_{\rm adv} \approx \frac{T_{\rm rms}V}{\kappa\Delta/L} = \frac{VL}{\kappa}\frac{T_{\rm rms}}{\Delta} . \tag{8}$$

This assumption can be also justified by the fact that the horizontal temperature gradient in the middle height is mainly due the thermal plumes, not the background flow.

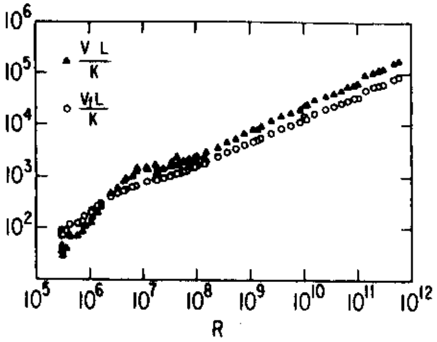

FIG 12. Free-fall velocity estimated by Eq. (7) is compared with the measured velocity (the data are taken from the D pair).

As we have measured the velocity V and temperature fluctuation $T_{\rm rms}$, we can compare the estimated free-fall velocity V_f expressed by Eq. (7) with measured velocity V. The results are presented in Fig. 12. They have a slight difference in scaling, $V_f/V \approx R^{-0.03}$ (the prefactor is of the order 1). We can also compare the estimated Nusselt number $N_{\rm adv}$ with the measured one N (Fig. 13); they have a scaling difference of $N_{\rm adv}/N \approx R^{0.03}$ (the prefactor is also of the order 1). In both figures, the estimated values and the directly measured data show almost the same evolution with the Rayleigh number. Obviously, there are some drawbacks in the above argument. In Eq. (7) we used the cell size L for the vertical length scale of the free fall, but this is only valid in the asymptotic limit, where the size of the boundary layer and mixing layer is negligible compared with L, which is not true near the onset of hard turbulence. Also, up to now we do not have information on velocity fluctuation and correlation between temperature and velocity.

The mechanism responsible for the large-scale background flow is still an open problem. The free-fall velocity discussed above is an estimation of the velocity for the thermal plumes, but not for the background flow. How the hot and cold plumes collectively induces this coherent flow is a nontrivial question. This phenomena might be related to meso-scale coherent structure in turbulent flow which is often observed in atmospheric phenomena.

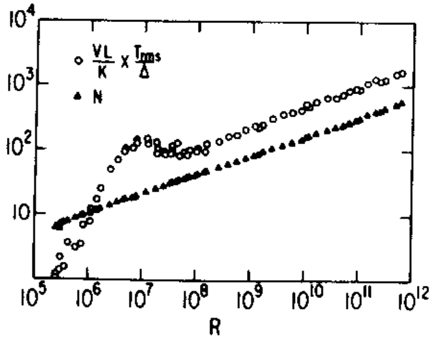

FIG. 13. Estimated Nusselt number by Eq. (8) is compared with the measured Nusselt number (the data for $T_{\rm rms}$ and V are taken from the bolometers of the D pair).

B. Prandtl number dependence

In this experiment, the change of the Prandtl number P (which is defined as the kinematic viscosity ν divided by the thermal diffusivity κ) is small. Specifically, P has a constant value of 0.64 for R up to 10^8, it changes gradually to 0.90 when R increases up to 10^{10}, and increases to 1.4 when R reaches 10^{12}. The Prandtl number dependence was neglected in the previous paper.[3] Although changes in Prandtl number in this experiment are small, that small variation can not be neglected when one wants to compare with the existing theories for velocity. For example, Garon and Goldstein[14] and, independently, Tanaka an Miyata[15] measured fluctuation of velocity and its scaling in water. According to Kraichnan's theory,[16] they assumed a Prandtl number dependence of velocity for high Prandtl number fluid ($P > 0.1$) as

$$\frac{V}{\kappa/L} \approx P^{1/3}R^{\beta} , \tag{9}$$

then found $\beta = 0.43$ for velocity fluctuation. If in our experiment we chose the same normalization of velocity, the scaling exponent for the large-scale flow velocity would be 0.46 ± 0.01. If we neglect the Prandtl number dependence, this exponent is 0.485 ± 0.005 as presented in Sec. III. However, the theoretical prediction[3,16] of scaling exponent was made for fluctuating velocity, but not for the mean velocity of the large-scale flow. We expect that a new experiment in a larger cell, covering the same range of Rayleigh numbers while keeping the Prandtl number constant, will solve this problem.

C. Transitions and the mechanism of the oscillations at the frequency ω_p

The mechanism that produces oscillations at the frequency ω_p was an open question in the previous paper.[3] In the present work we found that the phase of the cross spectrum of one of the D pair bolometers and the D' bolometer is 180° at ω_p within all the hard-turbulent regime. We also compared ω_p with the eddy circulation frequency for the large-scale flow, which is $V/4L$. Figure 14 shows the ratio of the two frequencies $\omega_p/(V/4L)$. The ratio is essentially one for a wide range of Rayleigh numbers (it is worthwhile to note that this ratio does not have any Prandtl number dependence). These two facts support a picture in which oscillations are connected to the large scale flow. The frequency ω_p is essentially decided by the circulation time of the large-scale flow. Feedback effects caused by the circulation can be one mechanism of the oscillation, but it is not sufficient to produce oscillation. The instability of the thermal boundary must be involved. Looking at the time series in hard turbulence near the side wall in Fig. 3(d), one notices that within the period of $1/\omega_p$ there exist two subperiods. One is a bursting period consisting of a train of cold (hot) bursts, which is followed by a laminar period. The bursting period corresponds to collective cold plumes, which may be generated by collective hot plumes arriving at and destabilizing the top boundary layer. The laminar period may correspond to a restoring period of the thermal boundary layer. In order to produce the next bursts at the circulating frequency, the necessary condition is that the restoring time of the boundary layer is shorter than the circulation time. This means that the diffusion time of the thermal boundary layer $\tau_{\rm diff} = \delta^2/\kappa$ (where δ is the thermal boundary layer thickness) has to be smaller than the passage time of the large scale flow $\tau_{\rm conv} = L/V$. Their ratio can be estimated from our measured data as follows:

$$\frac{\tau_{\rm diff}}{\tau_{\rm conv}} = \frac{\delta^2/\kappa}{L/V} = \frac{VL}{4\kappa}N^{-2} , \tag{10}$$

noting $N = L/2\delta$. Figure 15 shows this quantity as a function of Rayleigh number. The ratio is a monotonic decreasing function of Rayleigh number in hard-turbulence regime and it is consistently smaller than 1. It is worth noting another aspect of Fig. 15. If a thermal plume has a length scale comparable to the boundary layer thickness, $\tau_{\rm diff}$ also express the life time of a plume. In that case $\tau_{\rm conv}$ corresponds to a transit time of a plume i.. the side-wall region which is advected with large-scale flow. If the ratio is large enough, most of the plumes are connected from the bottom (top) boundary layer to top (bottom) boundary layer. On the other hand, if it is small enough, plumes are disconnected like droplet and can not reach the opposite boundary. This is a possible mechanism of the transition from soft to hard turbulence.

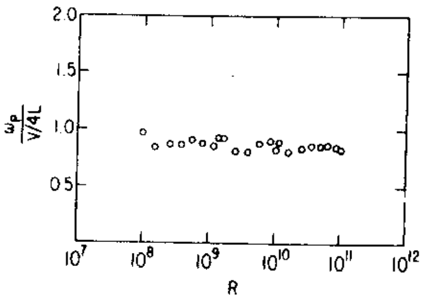

FIG. 14. Ratio between the oscillation frequency ω_p and the circulation frequency of large-scale flow $V/4L$ (the data for V are taken from the D pair).

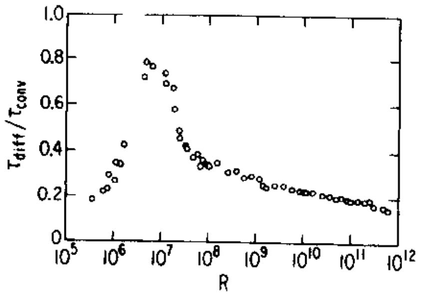

FIG. 15. Ratio between two time scales $\tau_{\rm conv} = L/V$ and $\tau_{\rm diff} = \delta^2/\kappa$ based on Eq. (10) (the data for V are taken from the D pair).

VII. CONCLUSION

The large-scale coherent flow is an important feature of the states of turbulence in this small aspect ratio cell. The measurement of the velocity and the horizontal temperature difference at middle height confirmed the preceding classification[2] of the various turbulent states. In this context, it is illuminating to look at Figs. 3 and 9.

The hard-turbulence state consists of a stable coherent flow around the cell with the emission of thermals from the boundary layer [cold fluctuation in Figs. 3(d) and 9(c′)]. The stem of the thermals are connected to the thermal boundary layer and advected horizontally by the large-scale flow,[8] which stretch them on the ascending and descending region of the flow. The center region [Figs. 9(c) and 9(d)] experiences only pinched off caps of the thermals. This thus defines a mixing length, average size of connected thermals, a center region, and a side region where the thermals and the coherent flow are on average parallel. In the hard-turbulence regime all the measured quantities, including the large-scale velocity and the horizontal temperature gradient, scale with Rayleigh number. The proposed scaling model[3] does not include the Prandtl number dependence, a necessary parameter for this experiment at large Rayleigh numbers.

Contrary to this model, the states of soft turbulence are associated with instabilities of the vertical motion of the coherent flow. Figures 3(a), 3(b) and 3(c) show that in those states the sign of fluctuation is opposite to the one in hard turbulence [Fig. 3(d)]. It indicates that the descending flow experiences large fluctuations at the bottom of the cell, where it is subjected to an opposing pressure field. Those states of turbulence are thus more complex, not universal, and geometry dependent.

We have also started to study the microscopic aspect of the turbulent states, by looking at the fast Fourier transform of the local temperature field. The main conclusion for the hard-turbulence state is in agreement with our earlier observations,[2] and is illustrated in Figs. 10(a) and 10(b). For a moderate Rayleigh number ($10^8 < R < 10^{11}$), the power spectrum in the side-wall region shows a power-law dependence with frequency, but its exponent increases with R (Fig. 11). But for larger R number ($R > 10^{11}$), a different power law develops at low frequency, starting at ω_p, with an exponent close to 1.4 and Rayleigh number independent [Fig. 10(b)]. For the larger Rayleigh number it can extend to more than one decade (in recent experiments performed where the Rayleigh number exceeds 10^{14}, this power law is present in the center and side of the cell on more than one decade of frequency). Those results warrant further experiments, including correlation with distance.

ACKNOWLEDGMENTS

We would like to thank B. Castaing, L. P. Kadanoff, and V. Yakhot for illuminating discussions and useful suggestions. We wish to thank Professor Hildebrand and NASA for providing the bolometers. This work has been supported by the National Science Foundation under Contract No. DMR 8722714 and one of us (M.S.) has been supported by the Japanese Society for Promotion of Science.

---

*Permanent address: The Research Institute of Electrical Communication, Tohoku University, Sendai 980, Japan.

[1] D. C. Threlfall, Ph.D thesis, University of Cambridge, 1976 (unpublished); J. Fluid Mech. **67**, 17 (1975).

[2] F. Heslot, B. Castaing, and A. Libchaber, Phys. Rev. A **36**, 5870 (1987).

[3] B. Castaing, G. Gunaratne, F. Heslot, L. Kadanoff, A. Libchaber, S. Thomae, X. Z. Wu, S. Zaleski, and G. Zanetti, J. Fluid Mech. **204**, 1 (1989).

[4] X. Z. Wu, B. Castaing, F. Heslot, and A. Libchaber, in *Universalities in Condensed Matter*, Vol. 32 of *Springer Proceedings in Physics* (Springer-Verlag, Berlin, 1988), p. 208.

[5] W. V. R. Malkus, Proc. R. Soc. London Ser. A **225**, 196 (1954); for an outline of a theory of turbulent convection, see *Theory and Fundamental Research in Heat Transfer*, edited by J. A. Clark (Pergamon, New York, 1963).

[6] L. N. Howard, in *Proceedings of the 11th International Congress of Applied Mechanics, Munich, 1966*, edited by Henry Goertler (Springer, Berlin, 1966), p. 1109.

[7] R. Krishnamurti and L. Howard, Proc. Natl. Acad. Sci. **78**, 4 (1981).

[8] S. Gross, G. Zocchi, and A. Libchaber, C. R. Acad. Sci. Paris **307**, 447 (1988).

[9] T. Y. Chu and R. J. Goldstein, J. Fluid Mech. **60**, 141 (1973).

[10] E. Reshotko, Ann. Rev. Fluid Mech. **8**, 311 (1976).

[11] For example, D. J. Tritton, *Physical Fluid Dynamics* (Van Nostrand, New York, 1977).

[12] A. N. Kolmogorov, C. R. Acad. Sci. USSR **30**, 301 (1941).

[13] D. E. Fitzjarrald, J. Fluid Mech. **53**, 643 (1976).

[14] A. M. Garon and R. J. Goldstein, Phys. Fluids **16**, 1818 (1973).

[15] H. Tanaka and H. Miyata, Int. J. Heat Mass Transfer **23**, 1273 (1980).

[16] R. H. Kraichnan, Phys. Fluids **5**, 1374 (1962).